

State Initialization of a Hot Spin Qubit in a Double Quantum Dot by Measurement-Based Quantum Feedback Control

A. Aarab,¹ R. Azouit,¹ V. Reiher,¹ and Y. Bérubé-Lauzière^{1,*}

¹*Institut quantique and Département de génie électrique et de génie informatique, Faculté de génie, Université de Sherbrooke, Sherbrooke, Québec, J1K 2R1, Canada*

A measurement-based quantum feedback protocol is developed for spin state initialization in a gate-defined double quantum dot spin qubit coupled to a superconducting resonator. The protocol improves qubit state initialization as it is able to robustly prepare the spin in shorter time and reach a higher fidelity, which can be pre-set. Being able to pre-set the fidelity aimed at is a highly desired feature enabling qubit initialization to be more deterministic. The protocol developed herein is also effective at high temperatures, which is critical for the current efforts towards scaling up the number of qubits in quantum computers.

I. INTRODUCTION

Since Loss and DiVincenzo's initial proposal of a quantum computing architecture relying on spin states in coupled single-electron quantum dots [1], important and steady efforts have been devoted in developing electron spin qubits both in research laboratories [2–6] and in industry with major players like Intel [7, 8] and IBM [9, 10]. The possibility with electron spin qubits to reach long coherence times on the order of seconds in silicon [2, 3, 11, 12], along with their spatial compactness and the exquisitely developed fabrication capabilities of the silicon industry, make them great candidates for physical qubit implementations.

To execute quantum algorithms, one of the key requirements for a qubit according to the DiVincenzo criteria [13] is the ability to initialize its state to a known quantum state, typically corresponding to the qubit's ground state and denoted $|0\rangle$. In practice, it is necessary that qubit initialization be robust, *i.e.* performed with high fidelity. This typically requires initialization to be carried out on a short timescale relative to the qubit's decoherence time. In this respect, protocols have been developed with the aim of reducing the initialization time and improving the fidelity of the procedure.

In this work we develop and numerically evaluate a new approach for actively initializing a spin qubit with high fidelity in an architecture consisting of a Si/SiGe gate-defined double quantum dot (DQD) coupled to a microwave superconducting resonator (μ WSCr), which is reminiscent of circuit quantum electrodynamics (cQED). This DQD- μ WSCr architecture, as proposed in [4, 14, 15], is a promising candidate for the fabrication of two-dimensional arrays of qubits with the long-range spin-spin connectivity required for quantum information processing and error correction. Such connectivity, which remains a great challenge [16–18], is achieved in this architecture by exploiting microwave photons in resonators to mediate the long-range spin-spin interactions, as has been demonstrated for superconducting qubits [19–21]. Using the large electric dipole of the electron charge state in a DQD through spin-charge hybridization, coherent interactions between single spins and microwave photons have already been demonstrated both theoretically [4] and experimentally [15, 22].

Several schemes for qubit initialization have been studied in cQED (see [23] and references therein). These systems can be initialized to the ground state via passive thermal relaxation (which has also been used for electron spin qubits in quantum dots [2, 24]), or some form of feedback conditioned on the outcome of a single-shot measurement [25–27]. These methods lead to limited fidelities and require operating temperatures in the tens to hundreds of mK.

Our approach to spin qubit active initialization relies on measurement-based quantum feedback made possible by the DQD- μ WSCr architecture which allows weak dispersive and quantum non-demolition (QND) measurements of the qubit's state via the resonator. We hereby present the design of a closed-loop control protocol to drive the qubit towards the desired initial state in a gradual and continuous manner.

With this approach, we show in a numerical comparative study that it is in principle possible to achieve higher qubit state initialization fidelities and shorter initialization times than with the current leading approaches mentioned above. This approach is also cheaper to implement experimentally as the qubit can be operated at temperatures up to 1 K and beyond while maintaining state initialization fidelities over 99.9%. Current efforts in scaling up spin qubit architectures [28–30] require on-chip control electronics that generate heat. Hence, initialization of spin qubits at higher temperatures [31–36], so-called hot qubits, is currently of very high interest.

The remainder of this paper is organized as follows: Sect. II presents the mathematical model of the DQD system considered herein comprising a spin and a charge degree of freedom, starting from the Hamiltonian and its eigenstates, incorporating its electrical interaction with a superconducting resonator, and presenting input-output theory of the compound system considered as an open quantum system. The spin and charge degrees of freedom of the DQD architecture are reduced to an effective two-level system, allowing to define a qubit and leading to an effective Jaynes-Cummings Hamiltonian describing the interaction between a qubit and a cavity as in cQED. Sect. III develops the model for dispersively measuring the qubit via the resonator, enabling weak QND measurements. Such measurements are essential for qubit state initialization relying on measurement-based quantum feedback, which is described in Sect. IV. Results of numerical simulations are presented in Sect. V, and Sect. VI concludes the paper.

* Corresponding author: Yves.Berube-Lauziere@USherbrooke.ca

II. DOUBLE QUANTUM DOT MODEL

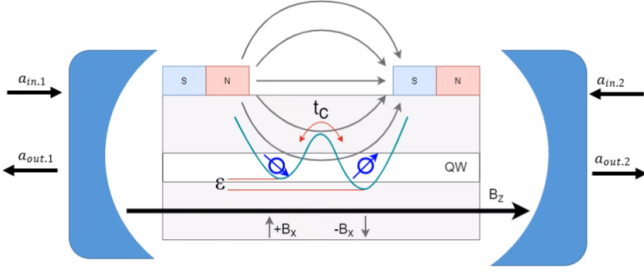


FIG. 1. Schematic representation of a DQD coupled to a cavity, adapted from Beniton *et al.* [4].

The system considered herein is that analyzed by Beniton *et al.* [4] and realized experimentally in [15], comprised of a gate-defined DQD coupled to a microwave superconducting resonator (Fig. 1). This DQD- μ WSCr system has a highly desired feature for the purpose of initializing a qubit state by measurement-based quantum feedback as considered here as it allows weak QND measurements of the qubit's state via measurement of the cavity's state. In what follows, we review for the sake of readability and completeness the salient features of the mathematical/physical model of the DQD- μ WSCr presented in [4] as pertinent for the present work.

The DQD (Fig. 1) confines a single electron in a gate-defined double electrostatic well. The spatial degree of freedom allows two basis states, for which the electron is located in the left (L) or right (R) dot (or well), with the possibility of the electron being in a superposition of these basis states. Depending on the applied gate voltages, there is a charging energy difference between the L and R dots to be denoted ϵ along with a tunnel coupling energy between the two dots denoted t_c . The DQD is subjected to an external longitudinal magnetic field B_z and a small transverse magnetic field gradient B_x . The B_z field separates the degenerate energy levels by Zeeman splitting. The B_x field gradient resulting from a micromagnet fabricated on top of the device induces spin-charge hybridization, which is required to achieve a strong spin-photon coupling with the microwave cavity [22, 37, 38]. The DQD Hamiltonian is given by:

$$H_0 = \frac{1}{2}(\epsilon\tau_z + 2t_c\tau_x + B_z\sigma_z + B_x\tau_x\sigma_z). \quad (1)$$

This is a four-level system, where the τ and σ operators are respectively Pauli operators pertaining to the electron's spatial and spin degrees of freedom. Since the spatial degree of freedom is related to the charge's position in the double well, it is also referred to as the charge degree of freedom. A qubit can be defined using a two-level subspace of this system. In occupation number formalism, the L and R basis spatial states are defined as $|L\rangle = |1, 0\rangle$ and $|R\rangle = |0, 1\rangle$, where the number appearing left in the ket is the occupation of the DQD's left site and the number appearing right is the occupation of the right site. The spatial operators are given by: $\tau_z = |L\rangle\langle L| - |R\rangle\langle R|$, and $\tau_x = |L\rangle\langle R| + |R\rangle\langle L|$.

The energy levels and eigenstates of the Hamiltonian will be needed in what follows. For $B_x = 0$, there is no spin-charge coupling, and the energy orbitals are given by:

$$|E_0^{(0)}\rangle = |-, \downarrow\rangle, |E_1^{(0)}\rangle = |+, \downarrow\rangle, |E_2^{(0)}\rangle = |-, \uparrow\rangle, |E_3^{(0)}\rangle = |+, \uparrow\rangle. \quad (2)$$

Here, superscript (0) indicates that these are the eigenstates for $B_x = 0$, and the states $|\pm\rangle$ are the eigenstates of the bare DQD Hamiltonian $H_{\text{DQD,bare}} = \frac{1}{2}(\epsilon\tau_z + 2t_c\tau_x)$ with respective eigenvalues $E_{\pm} = \pm\frac{1}{2}\Omega$, where $\Omega = \sqrt{\epsilon^2 + 4t_c^2}$ is the so-called "orbital energy". Explicitly, these eigenstates are given by

$$|-\rangle = \frac{-(\cos\frac{\theta}{2} - \sin\frac{\theta}{2})|L\rangle + (\cos\frac{\theta}{2} + \sin\frac{\theta}{2})|R\rangle}{\sqrt{2}}, \quad (3)$$

$$|+\rangle = \frac{(\cos\frac{\theta}{2} + \sin\frac{\theta}{2})|L\rangle + (\cos\frac{\theta}{2} - \sin\frac{\theta}{2})|R\rangle}{\sqrt{2}}, \quad (4)$$

where $\theta = \arctan\frac{\epsilon}{2t_c}$, the so-called "orbital angle".

For $B_x \neq 0$, the energy levels can be obtained exactly analytically and are as follows in ascending order (the calculations pose no difficulty, but are lengthy):

$$E_0 = -\frac{1}{2}\left[\left(\Omega + \sqrt{B_z^2 + B_x^2\sin^2\theta}\right)^2 + B_x^2\cos^2\theta\right]^{\frac{1}{2}}, \quad (5)$$

$$E_1 = -\frac{1}{2}\left[\left(\Omega - \sqrt{B_z^2 + B_x^2\sin^2\theta}\right)^2 + B_x^2\cos^2\theta\right]^{\frac{1}{2}}, \quad (6)$$

$$E_2 = \frac{1}{2}\left[\left(\Omega - \sqrt{B_z^2 + B_x^2\sin^2\theta}\right)^2 + B_x^2\cos^2\theta\right]^{\frac{1}{2}}, \quad (7)$$

$$E_3 = \frac{1}{2}\left[\left(\Omega + \sqrt{B_z^2 + B_x^2\sin^2\theta}\right)^2 + B_x^2\cos^2\theta\right]^{\frac{1}{2}}. \quad (8)$$

Analytical expressions for the associated energy eigenstates $|E_0\rangle$, $|E_1\rangle$, $|E_2\rangle$, and $|E_3\rangle$ are much more difficult to obtain analytically. Rather, first order stationary perturbation theory is resorted to, which is justified for the present purposes since $B_x \ll B_z$. To apply perturbation theory, the Hamiltonian is written as

$$H_0 = H_z + H_x, \quad (9)$$

where $H_z = H_0(B_x = 0)$ is the Hamiltonian with $B_x = 0$, and $H_x = \frac{1}{2}B_x\tau_x\sigma_z$ is the perturbation caused by the magnetic field B_x and responsible for spin-charge hybridization. The H_x term can be considered small compared to the elements of the H_z matrix, since $B_x \ll B_z$. To first order, the eigenstates are then given by:

$$|E_n^{(1)}\rangle = |E_n^{(0)}\rangle + \sum_{k \neq n} |E_k^{(0)}\rangle \frac{\langle E_k^{(0)} | H_x | E_n^{(0)} \rangle}{E_n^{(0)} - E_k^{(0)}}, \quad (10)$$

where $|E_k^{(0)}\rangle$ and $|E_n^{(0)}\rangle$ are the eigenstates of H_z . This leads to

the energy eigenstates to first order (not normalized):

$$|E_0^{(1)}\rangle = |-, \downarrow\rangle + \frac{B_x \sin \theta}{2B_z} |-, \uparrow\rangle + \frac{B_x \cos \theta}{2(B_z + \Omega)} |+, \uparrow\rangle, \quad (11)$$

$$|E_1^{(1)}\rangle = |-, \uparrow\rangle - \frac{B_x \sin \theta}{2B_z} |-, \downarrow\rangle + \frac{B_x \cos \theta}{2(\Omega - B_z)} |+, \downarrow\rangle, \quad (12)$$

$$|E_2^{(1)}\rangle = |+, \downarrow\rangle - \frac{B_x \cos \theta}{2(\Omega - B_z)} |-, \uparrow\rangle - \frac{B_x \sin \theta}{2B_z} |+, \uparrow\rangle, \quad (13)$$

$$|E_3^{(1)}\rangle = |+, \uparrow\rangle - \frac{B_x \cos \theta}{2(B_z + \Omega)} |-, \downarrow\rangle + \frac{B_x \sin \theta}{2(B_z + \Omega)} |+, \uparrow\rangle. \quad (14)$$

Since $B_x \ll 2B_z$, the eigenstates can be further simplified to:

$$|E_0^{(1)}\rangle = |-, \downarrow\rangle, \quad (15)$$

$$|E_1^{(1)}\rangle = \cos \frac{\Phi}{2} |-, \uparrow\rangle + \sin \frac{\Phi}{2} |+, \downarrow\rangle, \quad (16)$$

$$|E_2^{(1)}\rangle = \sin \frac{\Phi}{2} |-, \uparrow\rangle - \cos \frac{\Phi}{2} |+, \downarrow\rangle, \quad (17)$$

$$|E_3^{(1)}\rangle = |+, \uparrow\rangle, \quad (18)$$

where $\Phi = \arctan \frac{B_x \cos \theta}{\Omega - B_z}$ is the so-called "spin-orbit mixing angle". The latter states form the orbital basis in the presence of coupling.

To obtain a coupling between the spin and microwave photons (~ 10 GHz), the gap between the energy eigenstates must be of the order of $\geq 40 \mu\text{eV}$. The qubit can be defined on either the transition $E_0 \leftrightarrow E_1$ or the transition $E_0 \leftrightarrow E_2$, with E_0 being the ground state energy. Charge decoherence corresponds to the transition from the state $|+, \downarrow\rangle$ to the state $|-, \downarrow\rangle$.

To manipulate the qubit state with feedback control, it is essential to use weak QND measurements. Such measurements can be performed with the DQD coupled to a superconducting microwave cavity (Fig. 1). Such coupling of the DQD with a single quantized mode of frequency $\omega_c = 2\pi f_c$ within a cavity can be described by the following interaction term [4]:

$$H_I = g_c(a + a^\dagger)\tau_z, \quad (19)$$

where a and a^\dagger are respectively the bosonic annihilation and creation operators for cavity photons at frequency ω_c . The term $a + a^\dagger$ is proportional to the electric field within the cavity. In the eigenbasis of $H_0(B_x \neq 0)$, the interaction term H_I becomes non-diagonal and takes the following form:

$$H_I = g_c(a + a^\dagger) \sum_{n,m=0}^3 d_{n,m} \sigma_{nm}, \quad (20)$$

where the step operators $\sigma_{nm} = |E_n\rangle \langle E_m|$ correspond to the transitions between the energy levels of the DQD and $d_{n,m}$ are the dipole moments associated with these transitions. This coupling leads to a spin-photon coupling via spin-charge hybridization. The Hamiltonian for the cavity mode of frequency ω_c is given by

$$H_c = \omega_c a^\dagger a. \quad (21)$$

Hence the full Hamiltonian of the DQD coupled with the

quantized mode of the cavity is given by

$$H = H_0 + H_c + H_I. \quad (22)$$

The DQD coupled to the cavity is an open quantum system. Since the DQD qubit will be measured later on via a measurement of the transmission of the cavity driven at a frequency ω_R , the dynamics of this coupled system needs to be described. For this, input-output theory is used [39], which is based on the Heisenberg picture and the quantum Langevin equations. If the cavity frequency is close to the Zeeman frequency ($\omega_c \approx B_z$), the transition $E_0 \leftrightarrow E_3$ is off-resonance. In addition, σ_{03} satisfies $\dot{\sigma}_{03} = -(\frac{\gamma_c}{2})\sigma_{03}$, where γ_c is the charge decoherence rate; σ_{03} is not coupled to σ_{01} and σ_{02} . It can be shown [4] that the dynamical evolution of the operators a , σ_{01} and σ_{02} in the frame rotating at the driving frequency ω_R is governed by:

$$\dot{a} = i\Delta_0 a - \frac{\kappa}{2}a + \sqrt{\kappa_1}a_{in,1} - ig_c(d_{01}\sigma_{01} + d_{02}\sigma_{02}), \quad (23)$$

$$\dot{\sigma}_{01} = -i\delta_1 \langle \sigma_{01} \rangle - \gamma_c \sin^2 \frac{\Phi}{2} \sigma_{01} + \frac{\gamma_c}{2} \sin \Phi \sigma_{02} - ig_c d_{10} a, \quad (24)$$

$$\dot{\sigma}_{02} = -i\delta_2 \sigma_{02} - \gamma_c \cos^2 \frac{\Phi}{2} \sigma_{02} + \frac{\gamma_c}{2} \sin \Phi \sigma_{01} - ig_c d_{20} a. \quad (25)$$

Here,

$$\Delta_0 = \omega_R - \omega_c, \quad (26)$$

is the detuning of the driving field relative to the cavity frequency, $\delta_n = E_n - E_0 - \omega_R$, with ω_R being near-resonant to the $E_0 \leftrightarrow E_1$ transition; κ is the total cavity decay rate, $\kappa_1 = \kappa/2$ is the decay rate through the input port, and $a_{in,1}$ the incoming field into the cavity.

In what follows, it will be useful to reduce the spin and charge degrees of freedom to an effective two-level system. For this purpose, it is convenient to consider the orbital basis $|\pm\rangle \otimes |\uparrow\downarrow\rangle$, and introduce the operators $\sigma_\tau = |-, \downarrow\rangle \langle +, \downarrow|$ and $\sigma_s = |-, \downarrow\rangle \langle -, \uparrow|$ [4]. Here, indices τ and s respectively refer to the charge and spin degrees of freedom. It is seen that σ_τ is the charge flip operator and will be related to charge decoherence effects in the regime of operation considered herein, and σ_s is the spin-flip operator with the charge remaining in the $|-\rangle$ state. Through Eqs. (15)-(18), σ_s and σ_τ are related to σ_{01} and σ_{02} as follows

$$\sigma_{01} \approx \cos \frac{\Phi}{2} \sigma_s + \sin \frac{\Phi}{2} \sigma_\tau, \quad (27)$$

$$\sigma_{02} \approx \sin \frac{\Phi}{2} \sigma_s - \cos \frac{\Phi}{2} \sigma_\tau. \quad (28)$$

The evolution of the system can thus be described in the orbital basis by the following equations:

$$\dot{a} = i\Delta_0 a - \frac{\kappa}{2}a + \sqrt{\kappa_1}a_{in,1} + ig_c \cos \theta \sigma_\tau, \quad (29)$$

$$\dot{\sigma}_\tau = -i\Delta_\tau \sigma_\tau - \gamma_c \sigma_\tau + ig_c \cos \theta a + i \frac{B_x \cos \theta}{2} \sigma_s, \quad (30)$$

$$\dot{\sigma}_s = -i\Delta_s \sigma_s + i \frac{B_x \cos \theta}{2} \sigma_\tau, \quad (31)$$

with

$$\Delta_{\tau(s)} = +(-) \frac{\Omega - B_z}{2} - E_0 - \omega_R, \quad (32)$$

where Δ_τ and Δ_s are in the few GHz range.

To reduce the charge decoherence and maximize the spin-photon coupling, it is important that the dynamics of the charge be in a stationary mode ($\dot{\sigma}_\tau = 0$), which gives :

$$\begin{aligned} \dot{a} = & i(\Delta_0 + \Delta_\tau \eta \cos^2 \alpha) a - \frac{\kappa'}{2} a + \sqrt{\kappa_1} a_{in,1} \\ & + i \sin \alpha \cos \alpha \eta (\Delta_\tau + i\gamma_c) \sigma_s, \end{aligned} \quad (33)$$

$$\dot{\sigma}_s = -i(\Delta_s - \Delta_\tau \eta \sin^2 \alpha) \sigma_s - \gamma_s \sigma_s + i \sin \alpha \cos \alpha \eta (\Delta_\tau + i\gamma_c) a, \quad (34)$$

with

$$\eta = \frac{B_x^2/4 + g_c^2}{\Delta_\tau^2 + \gamma_c^2} \cos^2 \theta, \quad (35)$$

$$\alpha = \arctan \frac{B_x}{2g_c}, \quad (36)$$

and effective decay rates

$$\kappa' = \kappa + 2\gamma_c \eta \cos^2 \alpha, \quad (37)$$

$$\gamma_s = \gamma_c \eta \sin^2 \alpha. \quad (38)$$

Neglecting γ_c compared to Δ_τ ($\gamma_c = 100$ MHz, see Table I below, whereas Δ_s is in the GHz range), Eqs. (33) and (34) can be written as

$$\dot{a} = i\omega'_c a - \frac{\kappa'}{2} a + \sqrt{\kappa_1} a_{in,1} + i g_s \sigma_s, \quad (39)$$

$$\dot{\sigma}_s = -i \frac{\omega_q}{2} \sigma_s - \gamma_s \sigma_s + i g_s a \quad (40)$$

where

$$\omega'_c = \Delta_0 + \Delta_\tau \eta \cos^2 \alpha, \quad (41)$$

$$\frac{\omega_q}{2} = \Delta_s - \Delta_\tau \eta \sin^2 \alpha, \quad (42)$$

$$g_s = \sin \alpha \cos \alpha \eta \Delta_\tau. \quad (43)$$

Considering the input field mode $a_{in,1}$ and the effective decay rates κ' and γ_s , Eqs. (39) and (40) show that the dynamics of the operators a and σ_s are those of a two-level system coupled to a single-mode field described by an effective Jaynes-Cummings Hamiltonian given by

$$H_{JC} = \omega'_c a^\dagger a + \frac{\omega_q}{2} \sigma_z + g_s (a^\dagger \sigma_s + a \sigma_s^\dagger). \quad (44)$$

In other words, Eqs. (39) and (40) can be obtained from this effective Hamiltonian.

III. MEASUREMENTS

In the theory presented above, the Heisenberg picture was used. In this section, the Schrödinger picture, in which a state is specified by a time-evolving vector or density operator, will be used instead as it is easier to handle in the context of feedback control. To be able to implement quantum feedback, it is important that weak, and QND measurements be used to affect as little as possible the state of the qubit as it is being measured. This can be achieved with the qubit being coupled with the cavity in the dispersive regime, with the effective dispersive Hamiltonian given by [19]:

$$H_{\text{disp}} = (\omega'_c + \chi \sigma_z) a^\dagger a + \frac{(\omega_q + \chi)}{2} \sigma_z, \quad (45)$$

with $\chi = g_s^2/(\omega'_c - \omega_q)$. This Hamiltonian is an approximation of the Jaynes-Cummings model in the case of a large frequency detuning between the qubit and the cavity relative to the coupling strength g_s [40].

The two physical qubit states $|g\rangle$ and $|e\rangle$ serve as the logical qubit states. To measure a qubit in a general state $|\psi\rangle = c_g |g\rangle + c_e |e\rangle$, the cavity is first emptied and initialized in a coherent state $|\alpha\rangle$ (the α appearing here shall not be confused with the α appearing in Eq. (36)). The qubit and cavity are then entangled for a duration T_m under the unitary evolution of the dispersive Hamiltonian; T_m defines the measurement time. The combined qubit-cavity system state after the entanglement interaction is:

$$|\Psi\rangle = c_g |g\rangle \otimes |\alpha_g\rangle + c_e |e\rangle \otimes |\alpha_e\rangle. \quad (46)$$

This shows that it is possible to measure the state of the cavity after entanglement with the qubit and subsequently infer the qubit's state; the latter being thus measured indirectly via the cavity. Experimentally, a Josephson parametric converter (JPC) device can be used to perform such a measurement [41]. A JPC allows recording two output values (I_m, Q_m), which are used to determine the new qubit state after a measurement. The α 's of the coherent states appearing in Eq. (46) are related to the means of the output values \bar{I}_m and \bar{Q}_m as follows:

$$\alpha_g = -\bar{I}_m + i\bar{Q}_m, \quad (47)$$

$$\alpha_e = \bar{I}_m + i\bar{Q}_m, \quad (48)$$

whereby \bar{I}_m and \bar{Q}_m are related to each other and can be determined through the following relationships:

$$\bar{I}_m^2 + \bar{Q}_m^2 = \bar{n} \kappa T_m, \quad \frac{\bar{I}_m}{\bar{Q}_m} = \frac{\chi}{\kappa}, \quad (49)$$

with χ being the dispersive interaction strength, κ the cavity decay rate, and $\bar{n} = \frac{|\alpha|^2}{\kappa T_m}$. Using the density operator to specify the state of the qubit, and denoting that density operator before a measurement by ρ_{before}^q , the state after measurement of the

cavity is

$$\rho_{\text{after}}^q(I_m, Q_m) = \frac{M_{I_m, Q_m} \rho_{\text{before}}^q M_{I_m, Q_m}^\dagger}{\text{tr}(M_{I_m, Q_m} \rho_{\text{before}}^q M_{I_m, Q_m}^\dagger)}, \quad (50)$$

with

$$M_{I_m, Q_m} = \frac{e^{-\frac{(Q_m - \bar{Q}_m)^2}{4\sigma_m^2}}}{\sqrt{\pi}} \begin{bmatrix} e^{-\frac{(\bar{I}_m - I_m)^2}{4\sigma_m^2}} e^{i\frac{\bar{I}_m Q_m}{2\sigma_m^2}} & 0 \\ 0 & e^{-\frac{(\bar{I}_m + I_m)^2}{4\sigma_m^2}} e^{-i\frac{\bar{I}_m Q_m}{2\sigma_m^2}} \end{bmatrix}, \quad (51)$$

where $\sigma_m^2 = \frac{1}{2}$ is the fundamental quantum noise associated with a measurement in both quadratures I and Q .

Classical noise is also present in measurements and must be considered in addition to the fundamental quantum noise. For the measurements considered here, classical noise can be assumed to be Gaussian and zero mean with variance σ_c^2 in both quadratures [41]. Introducing the total observed variance $\sigma^2 = \sigma_c^2 + \sigma_m^2$ after an imperfect (so-called inefficient) measurement due to the classical noise, and defining the measurement efficiency as $\eta_m = \sigma_m^2/\sigma^2$, the qubit density operator after an inefficient measurement that delivers measurement values I_m and Q_m becomes

$$\rho_{\text{after}}^q(I_m, Q_m) = \frac{\int \int dI dQ P(I_m, Q_m|I, Q) M_{I, Q} \rho_{\text{before}}^q M_{I, Q}^\dagger}{\text{tr}(\int \int dI dQ P(I_m, Q_m|I, Q) M_{I, Q} \rho_{\text{before}}^q M_{I, Q}^\dagger)}. \quad (52)$$

Here the measurement operator $M_{I, Q}$ is that of Eq. (51) with I_m and Q_m replaced by I and Q (note, however, that the means \bar{I}_m and \bar{Q}_m remain as such in the expression of $M_{I, Q}$, as well as η_m), and

$$P(I_m, Q_m|I, Q) = \frac{\exp\left[-\frac{(I_m - I)^2}{2(1-\eta_m)\sigma^2}\right] \exp\left[-\frac{(Q_m - Q)^2}{2(1-\eta_m)\sigma^2}\right]}{2\pi(1-\eta_m)\sigma^2}. \quad (53)$$

The latter probability density accounts for the classical measurement noise ($\sigma_c^2 = \sigma^2 - \sigma_m^2 = (1-\eta_m)\sigma^2$). A value $\eta_m = 0.6$ will be used in what follows, which is experimentally realistic [41].

Including classical noise, the measurement values I_m and Q_m are Gaussian distributed with means \bar{I}_m and \bar{Q}_m and variance σ^2 . When the two Gaussian distributions N_{α_e} and N_{α_g} overlap, a weak measurement can be performed on the qubit, whereas two distributions that are well separated leads to a projective measurement of the qubit. The entangling time T_m is the important parameter controlling the overlap between the two distributions, and therefore the strength of the measurement, see Fig. 3 for two illustrative cases. For $T_m = 200$ ns, the overlap between the two distributions is large. In this case, when the qubit measurement is indirectly performed via the cavity, the qubit state is less disturbed and only a small amount of information about this state can be extracted. For $T_m = 2 \mu\text{s}$, the overlap between the two distributions is small (distributions apart), and when a measurement is performed, the qubit state is thereby strongly disturbed. In this case, the qubit after the measurement is in either the $|g\rangle$ or the $|e\rangle$ state and the quantum information encoded within the qubit state

prior to the measurement is destroyed; this is evidently not desirable for feedback control.

The diagonal form of the measurement operator M_{I_m, Q_m} with unequal diagonal elements shows that only the states $|g\rangle$ and $|e\rangle$ can be prepared by way of quantum feedback as it converges. The reason is that upon convergence, the qubit is repeatedly measured with very little control applied to it. Hence, only eigenstates of the measurement operators can be prepared with quantum feedback [42–44]. Fig. 4 shows results validating this in the present case. The validation process consists in measuring the qubit state in sequence a number of times defined as n_{rep} . When n_{rep} is large ($n_{\text{rep}} = 100$ is used here), the qubit ends up in either the state $|g\rangle$ or $|e\rangle$. The histograms in Fig. 4 were obtained with 10,000 runs of measurements, taking the final state of the qubit at the end of each run containing n_{rep} measurements. Fig. 4 (a) illustrates the case with no decoherence. The states $|g\rangle$ and $|e\rangle$ are equiprobable after measurement in this situation. Fig. 4 (b) depicts the results in the presence of decoherence (cavity and qubit). In this case, owing to decoherence, the qubit state is much more likely to be found in $|g\rangle$ after measurement.

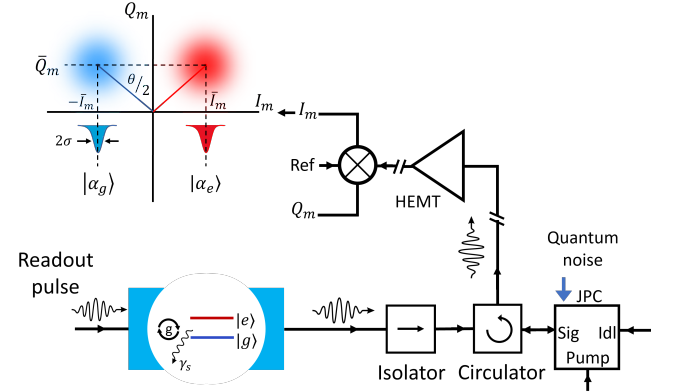


FIG. 2. Schematic illustration of the measurement chain of DQD in a cavity.

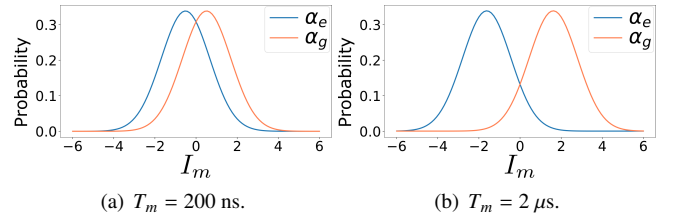


FIG. 3. The Gaussian distributions N_{α_e} and N_{α_g} .

IV. QUBIT STATE INITIALIZATION USING QUANTUM FEEDBACK CONTROL

The goal of control is to find a command signal to bring a system (the qubit here) to a desired state. The main advantage of feedback control is the ability to cope with uncertainty

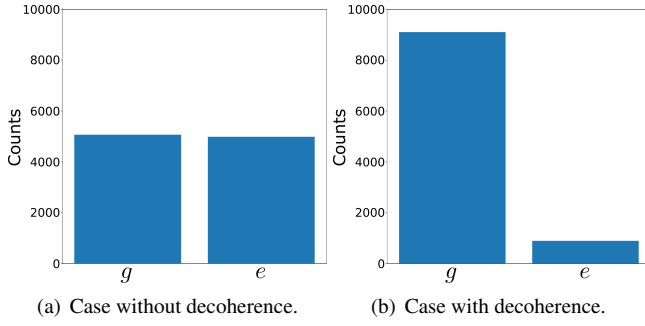


FIG. 4. Distribution of the states $|g\rangle$ and $|e\rangle$ in the validation process of the measurement operator.

and recover from unexpected events such as quantum jumps, noise, and measurement errors. This is achieved by monitoring the state of the system during control and adapting the command signal accordingly to reach the desired state.

It was demonstrated above that the equivalent two-level system serving as the qubit interacting with the cavity can be described by a Jaynes-Cummings Hamiltonian under appropriate conditions. A strong analogy can thus be established with cavity or circuit quantum electrodynamics (CQED). Hence control techniques inspired from those developed for CQED can be adapted. To control the qubit, it is assumed here that a general unitary gate having the form

$$U(\beta, \hat{n}) = \exp\left(-i\frac{\beta}{2}\hat{n} \cdot \vec{\sigma}\right) = \cos\frac{\beta}{2}I - i\sin\frac{\beta}{2}\hat{n} \cdot \vec{\sigma} \quad (54)$$

can be applied to its state, where β is the "spin rotation" angle and $\hat{n} = n_x\vec{i} + n_y\vec{j} + n_z\vec{k} \equiv (n_x, n_y, n_z)$ is a unit vector ($\|\hat{n}\| = 1$) specifying the axis around which the spin rotation takes place (\vec{i} , \vec{j} and \vec{k} are the unit vectors along the coordinates axes x , y and z). Hence, β and the direction specified by \hat{n} are the available parameters for control. In effect, the vector $\beta\hat{n}$ contains 3 independent parameters, and as will be seen below, it is those parameters that will be chosen appropriately for control. Such a unitary can be realized by way of electric dipole spin resonance (EDSR). For the DQD architecture considered here, EDSR can be implemented by subjecting the electron in the DQD to a longitudinal magnetic field (B_z in Fig. 1) and using gate voltages in the radio-frequency range applied to high frequency electrodes to move the electron back and forth from one dot to the other which makes it see an alternating transverse radio-frequency magnetic field along x as needed for EDSR [45].

Let ρ_m^q be the state of the qubit after a measurement and prior to applying the control via the gate U . Then, the state of the qubit ρ_c^q after applying the control is given by

$$\rho_c^q = U(\beta, \hat{n})\rho_m^q U^\dagger(\beta, \hat{n}). \quad (55)$$

One may object that if a general unitary gate is possible, then reaching any desired state with such a gate will be possible, and hence there is no need for feedback control. This is a simplistic view because this would require that the qubit be pre-

pared in an *a priori* known state before applying the gate, and that is exactly the problem addressed here, namely preparing that initial state. Furthermore, if an unexpected event occurs during state preparation, then there can be no guarantee that the desired state will be reached. Feedback control as considered here will thus consist in gradually bringing the state in a controlled way to the desired end state by monitoring its state during state preparation, and adapting the command signal as necessary. This is similar in spirit to the protocol devised by Serge Haroche's group to prepare Fock states in a microwave cavity [42, 43] as part of a CQED set-up. As mentioned previously, in the situation considered here, the cavity is used to gain information about the qubit's state in a QND manner and by least disturbing that state.

The control objective is to ultimately reach a state that has the smallest fidelity distance from the target state to be denoted ρ_{tag}^q . The fidelity distance $d_F(\rho_1, \rho_2)$ between two states ρ_1 and ρ_2 used here is defined as $d_F(\rho_1, \rho_2) = 1 - F(\rho_1, \rho_2)$, where $F(\rho_1, \rho_2) = \text{tr}(\rho_1\rho_2)$ is the fidelity. The control problem can thus be cast as minimizing the fidelity distance. Such minimization can be carried out iteratively by requiring that for each feedback loop (iteration), and given the information obtained about the state via a measurement made in the loop, the distance between the state ρ_c^q after the U gate is applied and the target state ρ_{tag}^q be smaller than the distance between the state prior to the application of the U gate, *i.e.* the state after measurement ρ_m^q , and the target state, that is

$$d_F(\rho_c^q, \rho_{\text{tag}}^q) < d_F(\rho_m^q, \rho_{\text{tag}}^q), \quad (56)$$

which, using Eq. (55), amounts to

$$\text{tr}(U\rho_m^q U^\dagger \rho_{\text{tag}}^q) > \text{tr}(\rho_m^q \rho_{\text{tag}}^q). \quad (57)$$

By developing to first order the left-hand side of the previous inequality for small values of β , in which case $U(\beta, \hat{n}) \approx I - i\frac{\beta}{2}\hat{n} \cdot \vec{\sigma}$, it is shown that this inequality is satisfied by choosing $\beta\hat{n}$, such that

$$\beta(n_x \text{tr}(i\sigma_x C) + n_y \text{tr}(i\sigma_y C) + n_z \text{tr}(i\sigma_z C)) > 0, \quad (58)$$

where C stands for the commutator given by $C = [\rho_{\text{tag}}^q, \rho_m^q]$. Defining the vector

$$\vec{v} = \text{tr}(i\sigma_x C)\vec{i} + \text{tr}(i\sigma_y C)\vec{j} + \text{tr}(i\sigma_z C)\vec{k}, \quad (59)$$

the condition in Eq. (58) is equivalent to $\beta\hat{n} \cdot \vec{v} > 0$. For this condition to be satisfied, β can be chosen positive and small, and \hat{n} can be taken as $\hat{n} = \vec{v}/\|\vec{v}\|$. More specifically as regards β , its value must be chosen sufficiently small such that when developing the left-hand side of the inequality in Eq. (57) in powers of β , the second order term in β is much smaller than the first order term to ensure that the inequality holds robustly to first order (for this calculation, $U(\beta, \hat{n})$ must be expanded up to second order in β). This leads to the following condition on β :

$$\beta \ll \zeta, \quad \text{with } \zeta = \left| \frac{\text{tr}(\vec{n} \cdot \vec{\sigma} C)}{\text{tr}(\vec{n} \cdot \vec{\sigma} \rho_m^q \vec{n} \cdot \vec{\sigma} \rho_{\text{tag}}^q) - \text{tr}(\rho_m^q \rho_{\text{tag}}^q)} \right|. \quad (60)$$

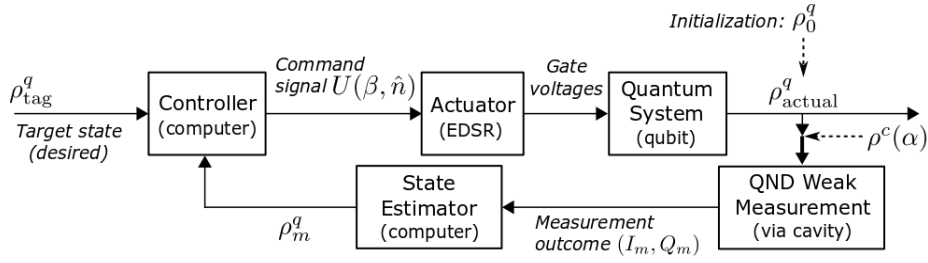


FIG. 5. Block diagram of the feedback protocol.

In practice, for the results presented below $\beta = \epsilon\zeta$, with $\epsilon = 0.1$ (the exact value of ϵ does not affect much the results, $\epsilon = 0.01$ has also been tested without significant changes in the results).

The feedback protocol of the qubit considered here is implemented in an iterative process similar to that presented in [42], and is depicted as a block diagram in Fig. 5. In this figure, the actuator is the physical interface that translates a computed command signal into a physical action that can physically be applied (typically in the form of fields) to the quantum system (qubit here) to control it. More specifically here, this physical interface consists in the radio-frequency voltages applied to the high frequency electrodes that allow EDSR. The feedback protocol starts from an initial *a priori* unknown qubit state ρ_0^q . As indicated in Fig. 5, this corresponds to ρ_{actual}^q being initialized to ρ_0^q . In each feedback loop (iteration), prior to measurement, the cavity is emptied and initialized to a coherent state $\rho^c(\alpha) = |\alpha\rangle\langle\alpha|$ as described in Section III (see also Fig. 5). The combined qubit-cavity state at this point is $\rho_{actual}^{q,c} = \rho_{actual}^q \otimes \rho^c(\alpha)$. To account for decoherence and thermal events affecting both the qubit and cavity, the free evolution of the combined state is modeled using a Lindblad master equation. In a real experiment this free evolution occurs by itself, but for the purpose of feedback control, it is also needed to model this evolution in order to obtain an estimate of the state for the calculating the command signal. The Lindblad equation accounts for: (i) the decoherence of the qubit (longitudinal and transverse relaxation), (ii) thermal excitation and relaxation of the qubit through interaction with the thermal environment at temperature T , (iii) relaxation of the cavity, and (iv) thermal excitation and relaxation of the cavity with the thermal environment. In the numerical modelling, this evolution takes place prior to measurement. This way of proceeding assumes that this free evolution accounts for all decoherence and thermal processes that may occur during a feedback loop iteration. Free evolution is defined here as evolution not caused by measurement back-action (Eq. (52)) or the action of control (Eq. (55)). A further underlying assumption for the sake of modelling is that no decoherence or thermal events occur while performing a measurement of the cavity, or during control action of the qubit. These assumptions, which are customary, ease the modelling process, although in reality, there can be decoherence and thermal events during a cavity measurement, or a control action. Such assumptions nevertheless provide for accurate and realistic modelling results as shown by the work of Haroche *et al.* in the case of controlling a mi-

crowave quantum cavity [42, 43], and are justified by the fact that decoherence and thermal events are stochastic. Hence, realistic modelling results are obtained by assuming that these events occur during a finite period of time in the course of a feedback loop, and apart from cavity measurement and qubit control action. The Lindblad equation for the combined (entangled) evolution of the qubit and cavity prior to measurement of the cavity in each feedback loop is given by:

$$\begin{aligned} \frac{d\rho^{q,c}}{dt} = & -i[H_{JC}, \rho^{q,c}] \\ & - \frac{\kappa'(1 + n_{th}(\omega_c))}{2} (a^\dagger a \rho^{q,c} + \rho^{q,c} a^\dagger a - 2a \rho^{q,c} a^\dagger) \\ & - \frac{\kappa' n_{th}(\omega_c)}{2} (a a^\dagger \rho^{q,c} + \rho^{q,c} a a^\dagger - 2a^\dagger \rho^{q,c} a) \\ & - \frac{\gamma_s(1 + n_{th}(\omega_q))}{2} (\sigma_s^\dagger \sigma_s \rho^{q,c} + \rho^{q,c} \sigma_s^\dagger \sigma_s - 2\sigma_s \rho^{q,c} \sigma_s^\dagger) \\ & - \frac{\gamma_s n_{th}(\omega_q)}{2} (\sigma_s \sigma_s^\dagger \rho^{q,c} + \rho^{q,c} \sigma_s \sigma_s^\dagger - 2\sigma_s^\dagger \rho^{q,c} \sigma_s), \end{aligned} \quad (61)$$

with $\rho^{q,c}(0) = \rho_{actual}^q \otimes \rho^c(\alpha)$, and where

$$n_{th}(\omega) = \frac{1}{e^{\hbar\omega/k_B T} - 1} \quad (62)$$

is the average number of thermal photons per mode at frequency ω given by Planck's law. The parameters used in H_{JC} appearing in Eq. (61) are those of the dispersive regime. The qubit and cavity evolve according to the previous Lindblad equation for a duration $T_m = 200$ ns (duration of a weak measurement as seen above). Following this evolution, the qubit is subjected to a QND weak measurement via an (I, Q) measurement of the cavity as previously described in Sect. III. The state of the qubit ρ_m^q indicated in Fig. 5 and following a measurement outcome I_m and Q_m is modeled using Eq. (52). This state is then compared by the controller against the target state using the fidelity distance. If this distance is small enough (*i.e.* smaller than a preset threshold), then the target state is considered to be reached. Otherwise, the controller computes the parameters β and \hat{n} of the control operator $U(\beta, \hat{n})$ as described above in order to reduce the fidelity distance. The operator $U(\beta, \hat{n})$ is then applied to the qubit by way of EDSR and another feedback iteration is initiated.

In this paper, the control protocol is developed and tested by way of numerical simulations. In a real experiment, the

sequence of modelling steps within a given feedback iteration described above defines a quantum filter [46, 47]. During an experiment, the exact state of the qubit cannot be known. However, a quantum filter, which provides a state estimator analogous to a Kalman filter in classical control theory, allows having a real-time estimate of the state of the qubit in the computer. This estimate enables computing the parameters β and \hat{n} of the control operator $U(\beta, \hat{n})$ to be applied at the end of the iteration as demonstrated by Haroche *et al.* [43]. Although prior to feedback the state of the qubit is unknown, accumulation of information on the qubit state via weak measurement outcomes over multiple feedback loops allows the filter to provide a faithful and reliable real-time representation of the qubit's real state irrespective of the initial state [42].

For clarity, each of the elementary operations on the qubit state (Lindblad evolution, weak measurement, and control) will be represented in what follows using the superoperator formalism [42, 48]. Hence, assuming ρ_{before}^q is the qubit state prior to an elementary operation and ρ_{after}^q is the state after that operation, then the general form of the equation representing the effect of that operation on state ρ_{before}^q to give state ρ_{after}^q will generally be written as $\rho_{\text{after}}^q = \mathbf{S}\rho_{\text{before}}^q$, where \mathbf{S} is the superoperator representing the operation. Using this formalism, the evolution of the qubit state resulting from the Lindblad evolution during a time T_m (Eq. (61)) is written as $\rho_{\text{after}}^q = \mathbf{L}(T_m)\rho_{\text{before}}^q$. Likewise, Eq. (52) for a measurement with outcome I_m , Q_m , will be written as $\rho_{\text{after}}^q = \mathbf{M}_{I_m, Q_m}\rho_{\text{before}}^q$. Finally, the action of the control unitary gate (Eq. (55)) takes the form $\rho_{\text{after}}^q = \mathbf{U}(\beta, \hat{n})\rho_{\text{before}}^q$. Summarizing, and provided that the state of the qubit is $\rho_{\text{begin}, j}^q$ at the beginning of the j -th iteration, the state of the qubit at the end of the iteration is given by:

$$\rho_{\text{end}, j}^q = \mathbf{U}(\beta_j, \hat{n}_j) \mathbf{M}_{I_{m_j}, Q_{m_j}} \mathbf{L}_j(T_m) \rho_{\text{begin}, j}^q. \quad (63)$$

This equation can be applied recursively at each iteration to get a real-time estimate of the state of the qubit. Starting from an initial qubit state ρ_0^q prior to feedback, the estimate of the state provided by the quantum filter at the end of iteration k ($k = 0$ corresponding to the initial state) is given by

$$\rho_{\text{end}, k}^q = \prod_{j=1}^k \mathbf{U}(\beta_j, \hat{n}_j) \mathbf{M}_{I_{m_j}, Q_{m_j}} \mathbf{L}_j(T_m) \rho_0^q. \quad (64)$$

As mentioned, feedback control loops are iteratively applied until convergence, *i.e.* until the fidelity distance reaches a value below a predetermined threshold value.

V. RESULTS

The target state for initialization is the qubit's ground state $|g\rangle$ considered to be the logical state $|0^q\rangle$. Note that given the qubit is in a state ρ^q , the probability of preparing the qubit's ground state $|\psi_{\text{tag}}^q\rangle = |0^q\rangle$ with corresponding density operator $\rho_{\text{tag}}^q = |0^q\rangle\langle 0^q|$ is the same as the fidelity since $F(\rho^q, \rho_{\text{tag}}^q) = \text{tr}(\rho^q \rho_{\text{tag}}^q) = \text{tr}(\rho^q |0^q\rangle\langle 0^q|) = \varphi(0)$.

Numerical results of qubit state initialization using the feedback approach described above will now be presented and compared to two other initialization approaches, namely thermal relaxation to the ground state and conditional feedback based on a single shot measurement. These two other approaches are considered as they can be performed with the DQD- μ WSCr architecture without any additional hardware such as a single electron transistor (SET) to measure the qubit. All numerical simulations have been performed using QuTip [49], and the parameters values used are provided in Table I. These values are experimentally realistic, and were taken from the literature [4, 15]. From Table I, the following values are computed (Eqs. (26), (35)-(38), (41)-(43)): $\omega_R = 5.855$ GHz, $\eta = 0.0156$, $\alpha = 78.46^\circ$, $\kappa' = 1.895$ MHz, and $\gamma_s = 1.501$ MHz, $\omega'_c = 6.02$ MHz, $\omega_q = -0.146$ GHz, and $g_s = 4.89$ MHz. The effective cavity and qubit frequencies ω'_c and ω_q are given with respect to the frame rotating at the cavity driving frequency ω_R . In the laboratory frame, ω_R needs to be added to these frequencies.

TABLE I. Parameter values used in the numerical simulations.

Parameter	Value	Unit
ε	0	μeV
t_c	15.4	μeV
B_z	24	μeV
B_x	1.62	μeV
g_c	40	MHz
γ_c	100	MHz
ω_c	5.85	GHz
κ	1.77	MHz
Δ_0	5	MHz

A. Thermal relaxation to the ground state

In thermal relaxation to the ground state, the qubit is assumed to be in an *a priori* unknown initial state and one waits sufficiently long for it to fall into its ground state [2, 24]. More precisely, once the probability of measuring the qubit in the ground state is sufficiently high, the qubit is considered initialized and can be used for a computation.

To model thermal relaxation along with decoherence of the qubit's state ρ^q , the following Lindblad equation is used

$$\begin{aligned} \dot{\rho}^q = & -\frac{i\omega_q}{2} [\sigma_z, \rho^q] \\ & - \frac{\gamma_s(1+n_{\text{th}})}{2} [\sigma_+ \sigma_- \rho^q + \rho^q \sigma_+ \sigma_- - 2\sigma_- \rho^q \sigma_+] \\ & - \frac{\gamma_s n_{\text{th}}}{2} [\sigma_- \sigma_+ \rho^q + \rho^q \sigma_- \sigma_+ - 2\sigma_+ \rho^q \sigma_-], \end{aligned} \quad (65)$$

from which the probability of the qubit being in the ground state at different times can be computed. Fig. 6 shows the results at 10 mK and 1 K for 100 initial states (pure and mixed) which were randomly sampled on and within the Bloch sphere to simulate an unknown initial state. These temperatures cor-

respond to realistic temperatures for experiments. At the very low temperature (10 mK), the qubit is initialized to the ground state with high probability after $3 \mu\text{s}$ irrespective of the initial state. A mean fidelity of 98.7% is obtained with a 95% confidence interval of [98.58, 98.82]. At the higher temperature (1 K), the approach fails reaching state $|0\rangle$ (mean initialization fidelity of 56.92% with a 95% confidence interval of [56.91, 56.93]).

This approach has two drawbacks. First, it requires very low temperatures to avoid thermal excitation once in the ground state. Second, even at very low temperatures, this approach is slow as it is limited by the longitudinal relaxation time T_1 ; optimizing this approach contradicts the requirement for qubits to have long coherence times.

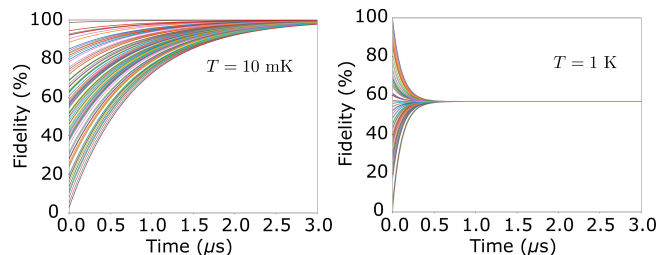


FIG. 6. Qubit state initialization with thermal relaxation to the ground state.

B. Conditional feedback based on a single shot measurement

Conditional feedback based on a single shot measurement consists in performing a QND projective, hence strong, measurement of the qubit and conditionally apply a π rotation depending on the measurement outcome [25–27]. If the qubit is measured in the ground state, then no action is taken and by the projection postulate the qubit is in the ground state. Else if the qubit is found in the excited state, then a π rotation is applied to bring the qubit to its ground state. Here a strong measurement is performed via the cavity with a measurement time $T_m = 2 \mu\text{s}$ (Gaussian distributions well separated, Sect. III). The same approach as in Sect. IV using the Lindblad equation is used for simulating decoherence and thermal effects during the measurement time T_m . Fig. 7 depicts the histograms obtained with conditional feedback. A mean fidelity of 97.14% with 95% confidence interval of [95.45, 98.82] is obtained at $T = 10 \text{ mK}$, and at $T = 1 \text{ K}$ the mean fidelity is 96.50% with a 95% confidence interval of [95.04, 98.14]. Simulations were also performed for a measurement time $T_m = 3 \mu\text{s}$ with a mean fidelity of 98.62% (95% confidence interval of [97.47, 99.77]) at 10 mK and mean fidelity of 98.51% (95% confidence interval of [97.47, 99.77]) at 1 K. Further extending the measurement time marginally improves fidelity.

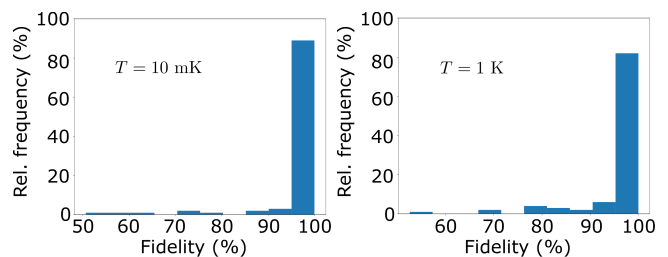


FIG. 7. Qubit state initialization with conditional feedback based on a single-shot measurement.

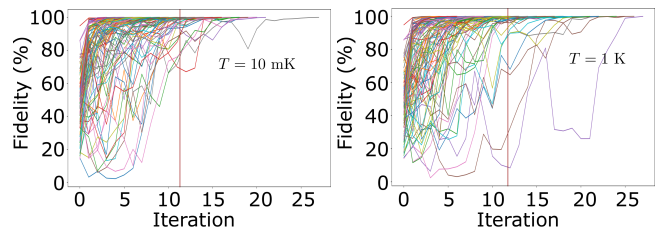


FIG. 8. Fidelity as a function of feedback iterations.

C. Quantum Feedback Control

In initialization relying on measurement-based quantum feedback control (Sect. IV), a targeted fidelity can be fixed at the outset, which is a key advantage of this approach. Here, a fidelity of 99.9% is targeted. A weak measurement with $T_m = 200 \text{ ns}$ is performed in each feedback loop. Fig. 8 shows the results of the numerical simulations with the fidelity plotted as a function of the number of feedback iterations. For both temperatures (10 mK and 1 K), the mean number of iterations required to reach the target fidelity is 11 (95% confidence interval of [10, 12]), corresponding to a mean initialization time of $2.2 \mu\text{s}$. This is shorter than the other two approaches considered above and, this, for a higher pre-set fidelity. The figure also illustrates that the feedback state initialization protocol is effective even in the presence of quantum jumps.

VI. CONCLUSIONS

In this work, a measurement-based quantum feedback protocol was developed for spin state initialization in an architecture relying on a gate-defined double quantum dot coupled to a superconducting resonator. This is a promising qubit building block for a spin-based quantum computer. Compared to two other initialization approaches relevant to this architecture, the protocol developed herein improves qubit state initialization as it is able to robustly initialize the spin in shorter time and reach a higher fidelity, which can be pre-set. The latter point is a highly desired feature as it provides for a more deterministic way of qubit initialization at a desired fidelity. It is to be noted that the coupling strength g_s considered here is only modestly greater than the decoherence rates γ_s and

κ' in current experimental realizations of the DQD- μ WSCr (see Table I and the values computed therefrom and Fig. 4d in Ref. [15]), and despite this the approach developed herein provides for fast high fidelity initialization. It can be expected that future improvements of the coupling strength, our initialization approach could even become faster. Furthermore, the protocol developed herein is effective at high temperatures, which is critical in current efforts to scale-up the number of qubits in quantum computers.

ACKNOWLEDGMENTS

This project was supported by Institut quantique at Université de Sherbrooke through the Canada First Research Excellence Fund. RA acknowledges financial support from a Prized Postdoctoral Fellowship from Institut quantique. VR acknowledges financial support via B1X - Bourses de maîtrise en recherche from the Fonds de recherche du Québec - Nature et technologies and Bourse VoiceAge pour l'excellence académique aux études supérieures from Université de Sherbrooke.

-
- [1] D. Loss and D. P. DiVincenzo, *Physical Review A* **57**, 120 (1998).
- [2] R. Hanson, L. P. Kouwenhoven, J. R. Petta, S. Tarucha, and L. M. K. Vandersypen, *Reviews of Modern Physics* **79**, 1217 (2007).
- [3] F. A. Zwanenburg, A. S. Dzurak, A. Morello, M. Y. Simmons, L. C. Hollenberg, G. Klimeck, S. Rogge, S. N. Copper-smith, and M. A. Eriksson, *Reviews of Modern Physics* **85**, 961 (2013).
- [4] M. Benito, X. Mi, J. M. Taylor, J. R. Petta, and G. Burkard, *Physical Review B* **96**, 235434 (2017).
- [5] L. M. K. Vandersypen and M. A. Eriksson, *Physics Today* **72**, 38 (2019).
- [6] A. Noiri, K. Takeda, T. Nakajima, T. Kobayashi, A. Sammak, G. Scappucci, and S. Tarucha, *Nature* **601**, 338 (2022).
- [7] R. Pillarisetty, N. Thomas, H. George, K. Singh, J. Roberts, L. Lampert, P. Amin, T. Watson, G. Zheng, J. Torres, M. Metz, R. Kotlyar, P. Keys, J. Boter, J. Dehollain, G. Droulers, G. Eenink, R. Li, L. Massa, D. Sabbagh, N. Samkharadze, C. Volk, B. P. Wuetz, A.-M. Zwerver, M. Veldhorst, G. Scappucci, L. Vandersypen, and J. Clarke, in *2018 IEEE International Electron Devices Meeting (IEDM)* (2018) pp. 6.3.1–6.3.4.
- [8] A. M. J. Zwerver, T. Krähenmann, T. F. Watson, L. Lampert, H. C. George, R. Pillarisetty, S. A. Bojarski, P. Amin, S. V. Amitonov, J. M. Boter, R. Caudillo, D. Corras-Serrano, J. P. Dehollain, G. Droulers, E. M. Henry, R. Kotlyar, M. Lodari, F. Luthi, D. J. Michalak, B. K. Mueller, S. Neyens, J. Roberts, N. Samkharadze, G. Zheng, O. K. Zietz, G. Scappucci, M. Veldhorst, L. M. K. Vandersypen, and J. S. Clarke, arXiv e-prints, arXiv:2101.12650 (2021), arXiv:2101.12650 [cond-mat.mes-hall].
- [9] A. V. Kuhlmann, V. Deshpande, L. C. Camenzind, D. M. Zumbühl, and A. Fuhrer, *Applied Physics Letters* **113**, 122107 (2018).
- [10] S. Geyer, L. C. Camenzind, L. Czornomaz, V. Deshpande, A. Fuhrer, R. J. Warburton, D. M. Zumbühl, and A. V. Kuhlmann, *Applied Physics Letters* **118**, 104004 (2021).
- [11] A. M. Tyryshkin, S. Tojo, J. J. Morton, H. Riemann, N. V. Abrosimov, P. Becker, H.-J. Pohl, T. Schenkel, M. L. Thewalt, K. M. Itoh, *et al.*, *Nature Materials* **11**, 143 (2012).
- [12] M. Veldhorst, J. Hwang, C. Yang, A. Leenstra, B. de Ronde, J. Dehollain, J. Muhonen, F. Hudson, K. M. Itoh, A. Morello, *et al.*, *Nature Nanotechnology* **9**, 981 (2014).
- [13] D. P. DiVincenzo, *Fortschritte der Physik: Progress of Physics* **48**, 771 (2000).
- [14] F. Beaudoin, D. Lachance-Quirion, W. Coish, and M. Pioro-Ladrière, *Nanotechnology* **27**, 464003 (2016).
- [15] X. Mi, M. Benito, S. Putz, D. M. Zajac, J. M. Taylor, G. Burkard, and J. R. Petta, *Nature* **555**, 599 (2018).
- [16] E. Chanrion, D. J. Niegemann, B. Bertrand, C. Spence, B. Jadot, J. Li, P.-A. Mortemousque, L. Hutin, R. Maurand, X. Jehl, *et al.*, *Physical Review Applied* **14**, 024066 (2020).
- [17] P.-A. Mortemousque, E. Chanrion, B. Jadot, H. Flentje, A. Ludwig, A. D. Wieck, M. Urdampilleta, C. Bauerle, and T. Meunier, arXiv preprint arXiv:1808.06180 (2018).
- [18] N. W. Hendrickx, W. I. Lawrie, M. Russ, F. van Riggelen, S. L. de Snoo, R. N. Schouten, A. Sammak, G. Scappucci, and M. Veldhorst, *Nature* **591**, 580 (2021).
- [19] A. Blais, R.-S. Huang, A. Wallraff, S. M. Girvin, and R. J. Schoelkopf, *Physical Review A* **69**, 062320 (2004).
- [20] A. Wallraff, D. I. Schuster, A. Blais, L. Frunzio, R.-S. Huang, J. Majer, S. Kumar, S. M. Girvin, and R. J. Schoelkopf, *Nature* **431**, 162 (2004).
- [21] L. DiCarlo, J. M. Chow, J. M. Gambetta, L. S. Bishop, B. R. Johnson, D. Schuster, J. Majer, A. Blais, L. Frunzio, S. Girvin, *et al.*, *Nature* **460**, 240 (2009).
- [22] J. Viennot, M. Dartiailh, A. Cottet, and T. Kontos, *Science* **349**, 408 (2015).
- [23] J. Tuorila, M. Partanen, T. Ala-Nissila, and M. Möttönen, *npj Quantum Information* **3**, 1 (2017).
- [24] R. Hanson, J. Elzerman, L. Willems van Beveren, L. Vandersypen, and L. Kouwenhoven, in *IEDM Technical Digest. IEEE International Electron Devices Meeting, 2004.* (2004) pp. 533–536.
- [25] D. Ristè, J. G. van Leeuwen, H.-S. Ku, K. W. Lehnert, and L. DiCarlo, *Physical Review Letters* **109**, 050507 (2012).
- [26] J. E. Johnson, C. Macklin, D. H. Slichter, R. Vijay, E. B. Weingarten, J. Clarke, and I. Siddiqi, *Phys. Rev. Lett.* **109**, 050506 (2012).
- [27] C. K. Andersen, J. Kerckhoff, K. W. Lehnert, B. J. Chapman, and K. Mølmer, *Phys. Rev. A* **93**, 012346 (2016).
- [28] M. Veldhorst, H. G. J. Eenink, C. H. Yang, and A. S. Dzurak, *Nature Communications* **8**, 1766 (2017).
- [29] R. Li, L. Petit, P. Franke David, P. Dehollain Juan, J. Helsen, M. Steudtner, N. K. Thomas, Y. Z. R., J. Singh Kanwal, S. Wehner, L. M. K. Vandersypen, J. S. Clarke, and M. Veldhorst, *Science Advances* **4**, eaar3960 (2018).
- [30] A. Ruffino, T.-Y. Yang, J. Michniewicz, Y. Peng, E. Charbon, and M. F. Gonzalez-Zalba, *Nature Electronics* **5**, 53 (2022).
- [31] L. M. K. Vandersypen, H. Bluhm, J. S. Clarke, A. S. Dzurak, R. Ishihara, A. Morello, D. J. Reilly, L. R. Schreiber, and M. Veldhorst, *npj Quantum Information* **3**, 34 (2017).

- [32] C. H. Yang, R. C. C. Leon, J. C. C. Hwang, A. Saraiva, T. Tanttu, W. Huang, J. Camirand Lemyre, K. W. Chan, K. Y. Tan, F. E. Hudson, K. M. Itoh, A. Morello, M. Pioro-Ladrière, A. Laucht, and A. S. Dzurak, *Nature* **580**, 350 (2020).
- [33] L. Petit, H. G. J. Eenink, M. Russ, W. I. L. Lawrie, N. W. Hendrickx, S. G. J. Philips, J. S. Clarke, L. M. K. Vandersypen, and M. Veldhorst, *Nature* **580**, 355 (2020).
- [34] J. Yoneda, W. Huang, M. Feng, C. H. Yang, K. W. Chan, T. Tanttu, W. Gilbert, R. C. C. Leon, F. E. Hudson, K. M. Itoh, A. Morello, S. D. Bartlett, A. Laucht, A. Saraiva, and A. S. Dzurak, *Nature Communications* **12**, 4114 (2021).
- [35] X. Xue, B. Patra, J. P. G. van Dijk, N. Samkharadze, S. Subramanian, A. Corna, B. Paquelet Wuetz, C. Jeon, F. Sheikh, E. Juarez-Hernandez, B. P. Esparza, H. Rampurawala, B. Carlton, S. Ravikumar, C. Nieva, S. Kim, H.-J. Lee, A. Sammak, G. Scappucci, M. Veldhorst, F. Sebastiano, M. Babaie, S. Pellerano, E. Charbon, and L. M. K. Vandersypen, *Nature* **593**, 205 (2021).
- [36] L. C. Camenzind, S. Geyer, A. Fuhrer, R. J. Warburton, D. M. Zumbühl, and A. V. Kuhlmann, *Nature Electronics* 10.1038/s41928-022-00722-0 (2022).
- [37] P.-Q. Jin, M. Marthaler, A. Shnirman, and G. Schön, *Phys. Rev. Lett.* **108**, 190506 (2012).
- [38] X. Mi, J. V. Cady, D. M. Zajac, P. W. Deelman, and J. R. Petta, *Science* **355**, 156 (2017), <https://www.science.org/doi/pdf/10.1126/science.aal2469>.
- [39] M. Collett and C. Gardiner, *Physical Review A* **30**, 1386 (1984).
- [40] S. Haroche and J.-M. Raimond, *Exploring the Quantum: Atoms, Cavities, and Photons* (Oxford University Press, 2006).
- [41] M. Hatridge, S. Shankar, M. Mirrahimi, F. Schackert, K. Geerlings, T. Brecht, K. M. Sliwa, B. Abdo, L. Frunzio, S. M. Girvin, R. J. Schoelkopf, and M. H. Devoret, *Science* **339**, 178 (2013).
- [42] I. Dotsenko, M. Mirrahimi, M. Brune, S. Haroche, J.-M. Raimond, and P. Rouchon, *Phys. Rev. A* **80**, 013805 (2009).
- [43] C. Sayrin, I. Dotsenko, X. Zhou, B. Peaudecerf, T. Rybarczyk, S. Gleyzes, P. Rouchon, M. Mirrahimi, H. Amini, M. Brune, and et al., *Nature* **477**, 73–77 (2011).
- [44] C. Guerlin, J. Bernu, S. Deléglise, C. Sayrin, S. Gleyzes, S. Kuhr, M. Brune, J.-M. Raimond, and S. Haroche, *Nature* **448**, 889–893 (2007).
- [45] M. Pioro-Ladrière, Y. Tokura, T. Obata, T. Kubo, and S. Tarucha, *Applied Physics Letters* **90**, 024105 (2007).
- [46] L. Bouten, R. van Handel, and M. R. James, *SIAM Journal on Control and Optimization (SICON)* **46**, 2199–2241 (2007).
- [47] L. Bouten, R. van Handel, and M. R. James, *SIAM Review* **51**, 239 (2009).
- [48] H. M. Wiseman and G. J. Milburn, *Quantum Measurement and Control* (Cambridge University Press, 2009).
- [49] J. Johansson, P. Nation, and F. Nori, *Computer Physics Communications* **184**, 1234 (2013).